JOURNAL OF Materials CHEMISTRY

Characterisation of nanoscopic $[Mn_{12}O_{12}(O_2CR)_{16}(H_2O)_4]$ single-molecule magnets: physicochemical properties and LDI- and MALDI-TOF mass spectrometry†

Daniel Ruiz-Molina,[a] Philippe Gerbier,[a] Evan Rumberger,[b] David B. Amabilino,[a] Ilia A. Guzei,[c] Kirsten Folting,[d] John C. Huffman,[d] Arnold Rheingold,[c] George Christou,*[d] Jaume Veciana*[a] and David N. Hendrickson*[b]

[a]*Institut de Ciència de Materials de Barcelona (CSIC), Campus Universitari, 08193 Bellaterra, Catalonia, Spain. Tel: 34 93 580 1853; Fax: 34 93 580 5729; E-mail: vecianaj@icmab.es*
[b]*Department of Chemistry and Biochemistry-0358, University of California at San Diego, La Jolla, California, 92093-0358, USA*
[c]*Department of Chemistry, University of Delaware, Newark, Delaware, 19716, USA*
[d]*Department of Chemistry and Molecular Structure Center, Indiana University, Bloomington, Indiana, 47405-4001, USA*

Received 25th May 2001, Accepted 11th January 2002
First published as an Advance Article on the web 8th February 2002

The syntheses of the two new single molecule magnets, $[Mn_{12}O_{12}(O_2CR)_{16}(H_2O)_4]S$ (R = $CHCHCH_3$, S = H_2O (**2**) and R = $C_6H_4C_6H_5$, S = $2C_6H_5C_6H_4COOH$ (**3**)) and X-ray crystal structure of the first are described. Complex **2** crystallizes in the orthorhombic space group *Ibca*, which at 198 K has a = 21.2208(4), b = 21.2265(4), c = 42.2475(6) Å, and Z = 8. Frequency-dependent out-of-phase ac signals are seen for both complexes, which indicates that these two complexes function as single-molecule magnets. Dc magnetization measurements for both complexes also exhibit hysteresis in the magnetization *vs.* external magnetic field plots with regular steps characteristic of quantum mechanical tunnelling of the direction of magnetization. The techniques of LDI- and MALDI-TOF mass spectrometry have been investigated to prospect their utility for the chemical characterization of Mn_{12} clusters. The technique is applied to known clusters as well as to two new compounds, and characteristic signals are found, especially predominant being that of the $[Mn_{12}O_{12}(O_2CR)_{14}]$ cation or anion, showing the potential interest of this technique for those preparing this type of compounds.

Introduction

The rapid growth of high-speed computers and the miniaturization of magnetic technology have led to much interest in the field of nanoscale magnetic materials.[1] In a nanomagnet there can be several domains where the spins within one domain are aligned and behave collectively because the spins are strongly coupled by magnetic exchange interactions. In response to an external magnetic field, domains sluggishly change the orientation of their magnetic moments to become aligned with the external magnetic field. As a consequence interesting magnetic properties such as magnetization hysteresis loops appear making such particles suitable candidates to be used as bits of information storage at the nanometer scale. Several synthetic methods have been developed to prepare these materials. One such technique is the fragmentation of bulk ferro- and ferri-magnetic materials. The main disadvantage of this "top-down" approach is that the nanoscale magnetic materials exhibit a distribution of particle size, anisotropy and shapes. This situation leads to a distribution of the barrier heights for the inter-conversion of the spins "up" to the spins "down" within the domains, which is not desirable for application in devices. From a fundamental point of view a distribution in barrier heights masks properties such as those associated with resonant magnetization tunnelling. Another technique involves growing crystallites of a known magnetic material in a micelle.[2] Since the size of the micelle cavity is tractable, predictable crystallite growth can be afforded. This method allows the synthesis of particles of controllable size, but thus far, has been limited to the miniaturization of known magnetic materials rather than the discovery of new structural classes of molecules.

The discovery of large metal cluster complexes with interesting magnetic properties characteristic of nanoscale magnetic particles, such as magnetization hysteresis loops and out-of-phase ac magnetic susceptibility signals, is an exciting breakthrough. Indeed, the advantages of using a synthetic approach (the so-called "bottom-up" approach) to obtain molecular nanomagnets are numerous: 1) metal clusters are normally prepared by a solution method and, once purified, are composed of single, sharply-defined size; 2) they are readily amenable to variations in peripheral ligands (small *vs.* bulky, hydrophilic *vs.* hydrophobic, *etc.*); 3) they are normally soluble in common solvents providing advantages in potential applications; 4) since each molecule has sub-nanoscale dimensions, such materials could potentially be used for high density information storage; and 5) from a theoretical point of view, understanding the magnetic properties of these molecules is important to help bridge the gap between the quantum and classical understanding of magnetism.[3]

In 1993 it was discovered for the first time that $[Mn_{12}O_{12}(O_2CCH_3)_{16}(H_2O)_4]\cdot 4H_2O\cdot 2CH_3CO_2H$ (**1**) (complex **1** or $Mn_{12}Ac$ for short), functions as a nanoscale molecular magnet.[4] Such a molecule has been termed a single-molecule

†LDI- and MALDI-TOF are acronyms for Laser Desorption/Ionisation and Matrix Assisted Laser Desorption/Ionisation Time-of-Flight.

 DOI: 10.1039/b104607c

magnet (SMM). This complex shows frequency-dependent out-of-phase ac magnetic susceptibility signals in the 4–7 K region for an ac field oscillating at frequencies in the range of 50–1000 Hz.[4] Pronounced hysteresis loops below 4 K, resulting from the slow magnetization relaxation rates, are also observed. However, the most interesting finding for the SMM's was made in 1996.[5] It was found that, in addition to thermal activation of each SMM over the barrier, the reversal of the direction of the magnetization also occurs *via* quantum mechanical tunnelling through the barrier. Since then, a few more families of complexes that function as SMM's have been obtained: 1) several other structurally related dodecanuclear manganese complexes, $[Mn_{12}O_{12}(O_2CR)_{16}(H_2O)_4]$ where R can be an aliphatic or aromatic group,[6–7] and their corresponding singly reduced salts (PPh_4)-$[Mn_{12}O_{12}(O_2CR)_{16}(H_2O)_4]$;[8] 2) several distorted Mn_4 cubane molecules with a $[Mn^{IV}Mn^{III}{}_3O_3X]^{6+}$ core,[9] 3) a mixed-valent complex $[Mn_4(O_2CMe)_2(Hpdm)_6][ClO_4]_2$[10] where Hpdm is the mono-anion of pyridine-2,6-dimethanol, and 4) tetranuclear vanadium(III) complexes with a butterfly structure.[11] A ferric complex $[Fe_8O_2(OH)_{12}(tacn)_6]^{8+}$, where tacn is triazacyclononane, has also been reported to display frequency-dependent out-of-phase peaks and magnetization hysteresis loops.[12]

Since the above discoveries, the interest to obtain new SMM's with precise chemical functionalities in order to achieve practical applications, larger dimensionalities and anisotropies, and high-spin ground states has grown considerably. One of the main limitations of this fascinating type of material has been found in their structural characterisation, where X-ray diffraction plays a crucial role. For this reason, the development of new techniques, such as mass spectrometry, to be used in routine characterization is very desirable. Among the various mass spectrometric techniques that can be used, matrix-assisted laser desorption/ionization time-of-flight mass spectrometry (MALDI-TOF MS)[13] has emerged as a particularly useful and efficient tool. MALDI-TOF MS has revolutionized the characterization of a wide range of high molecular weight natural[14] and synthetic polymers,[15] as well as nanoscopic organic molecules, such as dendrimers.[16] This "soft" mass spectrometric method, in which the molecular ionisation is provided by a pulse of (typically UV) laser light onto a sample, enables the observation of molecular ions of fragile molecules having masses in excess of 10^4 Daltons. While the technique is usually applied to purely organic molecules, in principle it is also useful for the characterization of inorganic compounds, and especially clusters. Indeed, the technique has found use in the characterization of rhenium(III) halides[17] as well as ruthenium[18] and osmium[19] carbonyl clusters. We hoped that the MALDI-TOF mass spectra of Mn_{12} clusters, with molecular weights ranging from 2000 to 4000 Daltons, would provide a simple characterization of these molecules.

In this work, we employ MALDI-TOF MS for the characterization of four single molecule magnets, the known $[Mn_{12}O_{12}(O_2CC_6H_5)_{16}(H_2O)_4]$ (**4**) and $[Mn_{12}O_{12}(O_2C\text{-}2\text{-}F\text{-}C_6H_4)_{16}(H_2O)_4]$ (**5**) and the two new SMM's $[Mn_{12}O_{12}(O_2CHCHCH_3)_{16}(H_2O)_4]\cdot H_2O$ (**2**) and $[Mn_{12}O_{12}(O_2CC_6H_4C_6H_5)_{16}(H_2O)_4]\cdot 2C_6H_5C_6H_4COOH$ (**3**). The magnetic properties of **2** and **3** and the X-ray structure of the former were determined. MALDI-TOF experiments of all the complexes under various experimental conditions, although not yet general, confirmed the utility of this spectrometric technique for measuring their molecular weights and composition.

Experimental section

Compound preparation. All chemicals and solvents were used as received; all preparations and manipulations were done under aerobic conditions. $[Mn_{12}O_{12}(O_2CMe)_{16}(H_2O)_4]\cdot 3H_2O\cdot CH_3COOH$ (**1**),[20] $[Mn_{12}O_{12}(O_2CC_6H_5)_{16}(H_2O)_4]$ (**4**)[6b] and $[Mn_{12}O_{12}(O_2C\text{-}2\text{-}F\text{-}C_6H_4)_{16}(H_2O)_4]$ (**5**)[21] were prepared as previously described.

$[Mn_{12}O_{12}(O_2CCHCHCH_3)_{16}(H_2O)_4]\cdot H_2O$ (2). To a slurry of complex **1** (1.0 g, 0.49 mmol) in 50 mL of toluene was added $HO_2CCHCHCH_3$ (1.49 g, 16 mmol). The solution was allowed to stir overnight. Then, the mixture was concentrated to remove the acetic acid. The resulting solid and additional $HO_2CCHCHCH_3$ (0.79 g, 8 mmol) were dissolved in toluene (50 mL), stirred overnight and then concentrated to remove acetic acid. To fully substitute the acetate ligands, this procedure was repeated once more. The resulting brown powder was recrystallized by slow diffusion of hexanes into a CH_2Cl_2 solution of the complex. The resulting brown crystals of $[Mn_{12}O_{12}(O_2CHCHCH_3)_{16}(H_2O)_4]\cdot H_2O$ (**2**) (70% yield based on total available $Mn_{12}Ac$) were collected on a frit and washed with hexanes. The crystals are suitable for structural determination by X-ray crystallography. Anal. Calcd. (Found) for $C_{64}H_{90}O_{49}Mn_{12}$: C, 33.38 (33.69); H, 3.95 (4.32)%.

$[Mn_{12}O_{12}(O_2CC_6H_4C_6H_5)_{16}(H_2O)_4]\cdot C_6H_5C_6H_4COOH$ (3). To a slurry of complex **1** (1.0 g, 0.49 mmol) in 50 mL of toluene was added $HO_2CC_6H_4C_6H_5$ (2.6 g, 13.3 mmol). The solution was allowed to stir overnight. Then, the mixture was concentrated to remove the acetic acid. The resulting solid and additional $HO_2CC_6H_4C_6H_5$ (1.3 g, 6.7 mmol) were dissolved in toluene (50 mL), stirred overnight and then concentrated to remove acetic acid. To fully substitute the acetate ligands, this procedure was repeated once more. The resulting brown powder was recrystallized by slow diffusion of hexanes into a CH_2Cl_2 solution of the complex. The resulting brown crystals of $[Mn_{12}O_{12}(O_2CC_6H_4C_6H_5)_{16}(H_2O)_4]\cdot 2C_6H_5C_6H_4COOH$ (70% yield based on total available $Mn_{12}Ac$) were collected on a frit and washed with hexanes. The crystals are not suitable for a publishable structural determination by X-ray crystallography. Anal. Calcd. (Found) for $C_{208}H_{152}Mn_{12}O_{48}$: C, 61.25 (61.29); H, 3.75 (3.91)%.

Crystallographic structural determination for complex 2. Crystal data collection, and refinement parameters are given in Table 1. The systematic absences in the diffraction data are uniquely consistent for the reported space group. An orthorhombic space group was chosen, despite the near equivalence of the *a* and *b* axis, because the systematic absences do not coincide with any *I*-centered tetragonal space group but are agreeable with the selected space group. The structure was solved by direct methods, completed by subsequent difference Fourier syntheses and refined by full-matrix least-squares procedures. The asymmetric unit of **2** contains half of the $[Mn_{12}O_{12}(O_2CHCHCH_3)_{16}(H_2O)_4]$

Table 1 Crystallographic data for $[Mn_{12}O_{12}(CH_3CHCHCOO)_{16}(H_2O)_4]\cdot H_2O$ (**2**)

Formula	$C_{64}H_{90}O_{49}Mn_{12}$
Formula weight	2302.64
Crystal system	Orthorhombic
Space group	*Ibca*
a, Å	21.2208(4)
b, Å	21.2265(4)
c, Å	42.2475(6)
V, Å^3	19030.1(7)
Z	8
Cryst. color, habit	Brown block
D(calc), g cm^3	1.607
μ(MoKα), cm^{-1}	16.24
Temp, K	198(2)
Diffractometer	Siemens P4/CCD
Rflns (collected, unique)	38823/7462
Radiation	MoKα(λ = 0.71073 Å)
$R(F)$, %[a]	7.77
$R(wF^2)$, %[a]	21.38

[a]Quantity minimized = $R(wF^2) = \Sigma[w(F_0^2 - F_c^2)^2/\Sigma[(wF_0^2)^2]^{1/2}$; $R = \Sigma\Delta/\Sigma(F_0)$, $\Delta = |(F_0 - F_c)|A$

complex, which lies on a 2-fold axis, and half of a water molecule. The alkyl carbon atoms in two of the crotonate ligands, C(21) to C(23) and C(41) to C(43), were fixed to an idealized carbon–carbon single bond distance. DIFABS[22] absorption corrections were applied. The disordered carbon atoms C(82) and C(83) and all non-hydrogen atoms were refined isotropically. The hydrogen atoms on the solvated water molecules of **2** were ignored. All other hydrogen atoms were refined as idealized contributions. All software and sources of the scattering factors are contained in the SHELXTL (5.10) program library (G. Sheldrick, Siemens XRD, Madison, WI). CCDC number 170659. See http://www.rsc.org/suppdata/jm/b1/b104607c/ for crystallographic files in .cif or other electronic format.

Physical measurements. Dc magnetic measurements were carried out on a Quantum Design MPMS SQUID magnetometer equipped with a 5.5 T magnet. The instrument has a 1.8–300 K operational range. Pascal's constants were used to subtract the diamagnetic contribution which then gave the molar paramagnetic susceptibilities. Magnetization hysteresis measurements were taken by suspending several crystals of complexes **2** or **3** in eicosane, heating the mixture to a temperature above the melting point of eicosane (313 K), subjecting the mixture to a 5.5 kOe field for 20 min, and then cooling the sample to room temperature. In this way, the crystals are oriented with their easy axis of magnetization parallel to the magnetic field. Samples prepared for variable field magnetization measurements were restrained in eicosane in a similar manner to prevent torquing. The computer program GENSPIN[23] was used to analyse variable-field magnetization data. The spin of the ground state is set at a value, and then the spin Hamiltonian matrix is diagonalised at each magnetic field to least-squares fit the experimental data. Ac susceptibility measurements were carried out on a Quantum Design MPMS2 SQUID ac magnetometer equipped with a 1 T magnet and a 1.7 to 400 K operational range. The instrument had a field range of 1×10^{-4} to 5 kOe and an oscillating frequency range of 5×10^{-4} to 1512 Hz.

LDI and MALDI-TOF MS. The mass spectra were recorded using a KRATOS ANALYTICAL (Manchester, UK) KOMPACT MALDI-2 K-PROBE instrument, which uses a 3 ns pulse from a nitrogen laser ($\lambda = 337$ nm) at a target area of 100 μm diameter, and pulse extracts the ions down a linear flight tube (2 m) in a vacuum of approximately 10^{-6} Torr. Spectra were run in positive and negative high mass mode, which employs a 20 kV pulsed extraction of the ions, typically accumulating 500 shots for each spectrum. The matrices 2-amino-4-methyl-5-nitropyridine (98%), the neutral 9-nitroanthracene (97%) and the slightly acidic dithranol (97%) were used as purchased from Aldrich Chemical Co. The samples were prepared by dissolving the cluster and matrix (at a concentration of 10 mg mL^{-1}) in an approximate 1 : 100 ratio in acetone or dichloromethane and then applying a 2 μL sample of the solution onto the stainless steel sample holders used in the instrument. The samples were run immediately after air drying at room temperature.

Results

Compound synthesis. The new complexes were synthesized from $[Mn_{12}O_{12}(O_2CMe)_{16}(H_2O)_4]\cdot 3H_2O\cdot CH_3COOH$ (**1**) by a ligand substitution reaction with the corresponding carboxylic acid,[24] as shown in Scheme 1.

This substitution reaction is a reversible reaction because the ligand strength of the replacement carboxylic and acetic acid are comparable. Two strategies have been used to drive the reaction to a fully complete substitution; i) add an excess of the desired carboxylic acid; and ii) remove the acetic acid from the system by vacuum distillation due to its lower boiling point relative to the other carboxylic acids. In any case, this substitution process has to be carried out several times to achieve complete substitution.

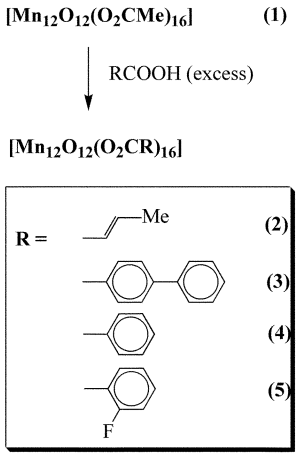

Scheme 1

Description of the X-ray structure. Complex **2** crystallizes in the *Ibca* space group. Crystallographic data are given in Table 1, and selected interatomic distances and angles are listed in Table 2. An ORTEP plot of complex **2** is presented in Fig. 1.

The complex possesses an $[Mn_{12}(\mu_3\text{-}O)_{12}]$ core comprising a central $[Mn^{IV}{}_4O_4]^{8+}$ cubane unit held within a nonplanar ring of eight Mn^{III} ions by eight $\mu_3\text{-}O^{2-}$ ions. This $[Mn_{12}(\mu_3\text{-}O)_{12}]$ core is essentially superimposable on the cores of other Mn_{12} complexes. Peripheral ligation is provided by sixteen carboxylate groups and four H_2O ligands. For all the complexes, the eight Mn^{III} ions fall into two groups of four Mn^{III} ions. In group I, each Mn^{III} ion is bonded to a single Mn^{IV} *via* two oxo bridges, while in group II each Mn^{III} is bonded to two Mn^{IV} *via* two oxo bridges. The four water ligands coordinate only to the four Mn^{III} ions of group II. For complex **2**, there are two H_2O ligands on one Mn^{III} atom of group II and two H_2O ligands bonded to another Mn^{III} atom of the same group. It is also interesting to emphasize that complexes **2** and **3** exhibit nanoscopic dimensions with diameters of 2.0 and 2.8 nm, respectively.

Magnetochemical characterization. Variable-temperature magnetic susceptibility data have been collected for the Mn_{12} complexes **2** and **3** in the temperature range of 5 to 320 K with an applied external field of 10.0 kOe. The samples were restrained in eicosane to prevent torquing. As an example, the plot of χT *vs.* T for complex **2** is depicted in Fig. 2.

At 320 K, complexes **2** and **3** are characterized by χT values of 21.7 and 20.0 cm^3 K mol^{-1}, respectively. These values are close to the spin-only value of 19.0 cm^3 K mol^{-1} expected for a cluster comprising 8 Mn^{III} and 4 Mn^{IV} non-interacting centers. From 320 to 120 K, the plots for both complexes show a gradual decrease whereupon χT increases rapidly until it reaches a maximum at 15 K with χT values of 55.4 and 56.0 cm^3 K mol^{-1} for complexes **2** and **3**, respectively. These values are close to the spin-only value expected for an $S = 10$ (55 cm^3 K mol^{-1}) ground state with $g = 2.0$.

Variable-field magnetic susceptibility data have been collected for the Mn_{12} complexes **2** and **3** in the range of 0.5–50 kG at low temperatures (2–30 K). The samples were restrained in eicosane to prevent torquing. In Fig. 3 is given a plot for complex **3** of the reduced magnetization, $M/N\mu_B$ where N is Avogadro's number and μ_B is the Bohr magneton, *versus* the ratio of the magnetic field divided by the absolute temperature (H/T).

Table 2 Selected bond lengths (Å) and angles (°) for $[Mn_{12}O_{12}(O_2CHCHCH_3)_{16}(H_2O)_4]\cdot H_2O$ (**2**)

Mn(1)-O(1)	1.868(8)	Mn(2)-O(7)	2.118(11)	Mn(4)-O(2)	1.900(7)	Mn(6)-O(20)	1.905(9)
Mn(1)-O(5)	1.872(9)	Mn(2)-O(7)	2.129(10)	Mn(4)-O(3)	1.910(9)	Mn(6)-O(5)	1.922(9)
Mn(1)-O(3)	1.904(8)	Mn(3)-O(14)	1.878(9)	Mn(4)-O(2)	1.929(7)	Mn(6)-O(19)	1.933(9)
Mn(1)-O(3)	1.908(8)	Mn(3)-O(6)	1.885(10)	Mn(4)-O(6)	1.851(9)	Mn(6)-O(21)	2.141(9)
Mn(1)-O(4)	1.928(9)	Mn(3)-O(13)	1.933(10)	Mn(5)-O(14)	1.913(9)	Mn(6)-O(22)	2.192(11)
Mn(1)-O(2)	1.944(8)	Mn(3)-O(11)	1.992(11)	Mn(5)-O(14)	1.913(9)	Mn(7)-O(5)	1.864(9)
Mn(2)-O(6)	1.902(10)	Mn(3)-O(15)	2.175(11)	Mn(5)-O(17)	1.959(10)	Mn(7)-O(5)	1.864(9)
Mn(2)-O(1)	1.907(9)	Mn(3)-O(6)	1.851(9)	Mn(5)-O(17)	1.959(10)	Mn(7)-O(23)	1.939(9)
Mn(2)-O(8)	1.954(9)	Mn(4)-O(14)	1.888(8)	Mn(5)-O(18)	2.223(10)	Mn(7)-O(23)	1.939(9)
Mn(2)-O(10)	2.002(12)	Mn(4)-O(16)	1.895(9)	Mn(5)-O(18)	2.223(10)	Mn(7)-O(24)	2.224(10)
				Mn(6)-O(1)	1.878(8)	Mn(7)-O(24)	2.224(10)
O(1)-Mn(1)-O(5)	85.0(4)	O(10)-Mn(2)-O(9)	87.7(4)	O(14)-Mn(4)-O(16)	93.6(4)	O(18)-Mn(5)-O(18)	175.3(6)
O(1)-Mn(1)-O(3)	91.2(4)	O(6)-Mn(2)-O(7)	92.9(4)	O(6)-Mn(4)-O(2)	92.8(4)	O(1)-Mn(6)-O(20)	97.2(4)
O(5)-Mn(1)-O(3)	89.6(4)	O(8)-Mn(2)-O(7)	85.5(4)	O(14)-Mn(4)-O(2)	89.6(3)	O(1)-Mn(6)-O(5)	83.3(4)
O(1)-Mn(1)-O(3)	174.2/4)	O(10)-Mn(2)-O(7)	86.5(5)	O(16)-Mn(4)-O(2)	174.1(4)	O(20)-Mn(6)-O(5)	176.8(4)
O(5)-Mn(1)-O(3)	98.1(4)	O(9)-Mn(2)-O(7)	173.5(4)	O(6)-Mn(4)-O(3)	98.1(4)	O(1)-Mn(6)-O(19)	175.5(4)
O(3)-Mn(1)-O(3)	84.0(4)	O(14)-Mn(3)-O(6)	82.7(4)	O(14)-Mn(4)-O(3)	174.2(3)	O(20)-Mn(6)-O(19)	84.6(4)
O(1)-Mn(1)-O(4)	92.7(4)	O(14)-Mn(3)-O(13)	94.4(4)	O(16)-Mn(4)-O(3)	92.0(4)	O(5)-Mn(6)-O(19)	92.6(4)
O(5)-Mn(1)-O(4)	94.9(4)	O(6)-Mn(3)-O(13)	173.6(4)	O(2)-Mn(4)-O(3)	84.7(3)	O(1)-Mn(6)-O(21)	92.6(4)
O(3)-Mn(1)-O(4)	174.3(4)	O(14)-Mn(3)-O(11)	175.4(4)	O(6)-Mn(4)-O(2)	176.0(4)	O(20)-Mn(6)-O(21)	89.4(4)
O(3)-Mn(1)-O(4)	91.9(4)	O(6)-Mn(3)-O(11)	95.6(4)	O(14)-Mn(4)-O(2)	97.5(4)	O(5)-Mn(6)-O(21)	93.7(4)
O(1)-Mn(1)-O(2)	96.1(4)	O(13)-Mn(3)-O(11)	86.8(4)	O(16)-Mn(4)-O(2)	91.3(4)	O(19)-Mn(6)-O(21)	91.6(4)
O(5)-Mn(1)-O(2)	173.2(4)	O(14)-Mn(3)-O(15)	95.3(4)	O(2)-Mn(4)-O(2)	83.3(4)	O(1)-Mn(6)-O(22)	85.2(4)
O(3)-Mn(1)-O(2)	83.7(4)	O(6)-Mn(3)-O(15)	96.2(4)	O(3)-Mn(4)-O(2)	80.6(3)	O(20)-Mn(6)-O(15)	96.2(4)
O(3)-Mn(1)-O(2)	80.3(3)	O(13)-Mn(3)-O(15)	89.8(4)	O(14)-Mn(5)-O(14)	96.2(5)	O(5)-Mn(6)-O(22)	86.0(4)
O(4)-Mn(1)-O(2)	91.7(4)	O(11)-Mn(3)-O(15)	89.1(4)	O(14)-Mn(5)-O(17)	90.2(4)	O(19)-Mn(6)-O(22)	90.6(4)
O(6)-Mn(2)-O(1)	94.0(3)	O(14)-Mn(3)-O(12)	87.6(4)	O(14)-Mn(5)-O(17)	173.6(4)	O(21)-Mn(6)-O(22)	177.8(4)
O(6)-Mn(2)-O(8)	174.4(4)	O(6)-Mn(3)-O(12)	86.9(4)	O(14)-Mn(5)-O(17)	173.6(4)	O(5)-Mn(7)-O(5)	94.7(5)
O(1)-Mn(2)-O(8)	91.5(4)	O(13)-Mn(3)-O(12)	87.2(4)	O(14)-Mn(5)-O(17)	90.2(4)	O(5)-Mn(7)-O(23)	92.1(4)
O(8)-Mn(2)-O(10)	81.9(4)	O(11)-Mn(3)-O(12)	88.0(4)	O(17)-Mn(5)-O(17)	83.4(6)	O(5)-Mn(7)-O(23)	173.2(4)
O(6)-Mn(2)-O(9)	90.4(5)	O(15)-Mn(3)-O(12)	176.0(4)	O(14)-Mn(5)-O(18)	89.7(4)	O(5)-Mn(7)-O(23)	92.1(4)
O(1)-Mn(2)-O(9)	91.4(4)	O(6)-Mn(4)-O(114)	83.4(4)	O(14)-Mn(5)-O(18)	93.4(4)	O(23)-Mn(7)-O(23)	81.2(6)
O(8)-Mn(2)-O(9)	90.7(5)	O(6)-Mn(4)-O(16)	92.5(4)	O(17)-Mn(5)-O(18)	87.0(5)	O(5)-Mn(7)-O(24)	86.9(4)

In the absence of zero-field splitting and at temperatures where only the ground state is populated, the $M/N\mu_B$ *vs.* H/T plots would follow the Brillouin function. It would also be expected that the $M/N\mu_B$ *vs.* H/T plots determined at different fields for a given complex would be superimposed. As can be seen in Fig. 3, even at 50.0 kG and 2.0 K the $M/N\mu_B$ value for complex **3** falls below the saturation values expected for a $S = 10$ ($M/N\mu_B = 20$) ground state with $g = 2$. Furthermore, the $M/N\mu_B$ *vs.* H/T plots determined at different fields do not superimpose, indicating that the ground state of these complexes is zero-field split. The $M/N\mu_B$ *vs.* H/T data were least-squares fit. Different minima differing in the ground state S and in the zero-field splitting parameter D, were located for each complex. The best fits were found to be $S = 10$, $D = -0.44$ cm^{-1}, and $g = 2.01$ for complex **2** and $S = 10$, $D = -0.33$ cm^{-1}, and $g = 1.73$ for complex **3**.

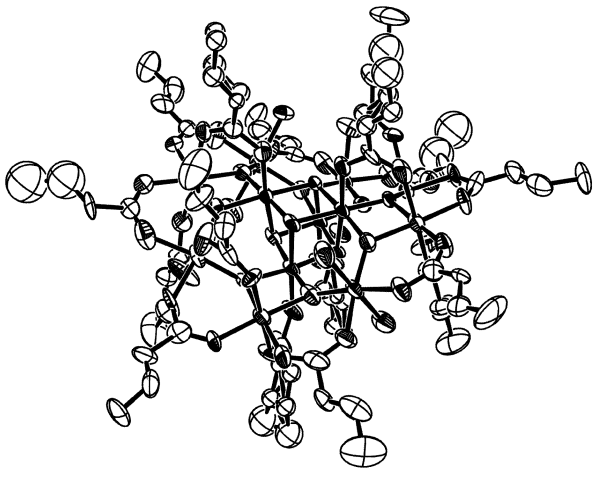

Fig. 1 Schematic diagram of $[Mn_{12}O_{12}(C_4H_5O_2)_{16}(H_2O)_4\ H_2O$ (**2**) showing atom labelling scheme. Water molecule and hydrogen atoms are omitted for clarity.

Magnetization hysteresis data were obtained for a few single crystals of complexes **2** and **3** at three temperatures in the range 1.8 to 2.5 K employing a SQUID magnetometer. The single crystals were oriented in eicosane such that the axial anisotropy axis of the molecule is parallel with the external field. The magnetic hysteresis loops collected for a few parallelly oriented single crystals of complex **2** are shown in Fig. 4 (upper panel). The sample was first magnetically saturated in a +2.0 T field, and then the field was swept down to −2.0 T, and cycled back to +2.0 T. As the field is decreased from +2.0 T to zero, there is the first step at zero field and successive steps are observed at a field interval of 4 kOe. If all the molecules changed their direction of magnetization by thermal activation over the barrier, then the hysteresis loop would be a smooth function with no steps. The steps are due to resonance quantum mechanical tunnelling of the magnetization direction.[6] In Fig. 4 are shown the magnetization hysteresis loops measured at 1.8, 2.0 and 2.5 K for complex **3** (lower panel). As can be seen, there

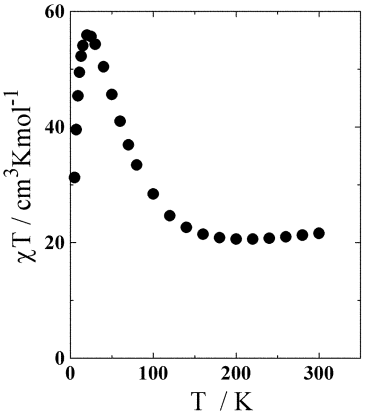

Fig. 2 Plot of $\chi_M \times T$ *vs.* temperature for complex **2** with an applied external field of 10.0 kOe(●).

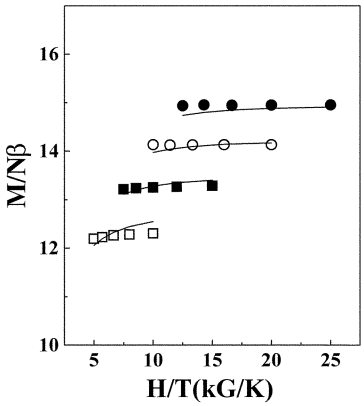

Fig. 3 Plot of the reduced magnetization, $M/N\mu_B$, where N is Avogadro's number and μ_B is the Bohr magneton, *versus* the ratio of the magnetic field divided by the absolute temperature (H/T) for complex **3**. Data were measured in the 2.0–4.0 K range for the magnetic fields of (●) 50 kOe, (○) 40 kOe, (■) 30 kOe and (□) 20 kOe.

are appreciable differences in step heights relative to the hysteresis loops collected for complex **2**. As the field is decreased from +2.0 T to zero, there is the first step at zero field, and successive steps are observed at a field interval of 5 kOe. The heights of these steps reflect the rate of magnetization tunnelling. Transverse zero-field and magnetic field interactions determine the rate of magnetization tunnelling. This rate is different in complexes **2** and **3** because these two complexes probably experience different magnitudes of transverse interactions. The different symmetry of the complexes probably influences the magnitude of the rhombic zero-field interaction $E(\hat{S}_x^2 - \hat{S}_y^2)$, which would lead to a difference in the rates of magnetization tunnelling. Single-crystal high-field EPR experiments would have to be carried out to determine the rhombic zero-field interaction E-parameters for these two complexes.

Ac magnetic susceptibility data were studied for polycrystalline samples of complexes **2** and **3** in the 1.8–10 K range with a 1 Oe ac field oscillating in the frequency range of 1–1150 Hz. The external dc magnetic field was held at zero. Frequency-dependent out-of-phase ac signals are seen for both complexes.

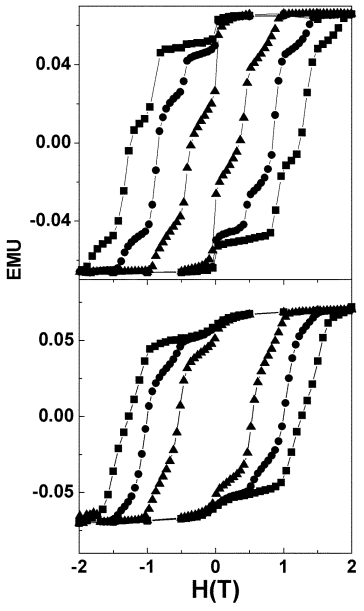

Fig. 4 Plots of magnetization *versus* external magnetic field for complex **2** (top trace) and complex **3** (bottom trace) at three temperatures in the 1.80–2.20 K range. Several small crystals were oriented in a frozen eicosane matrix so that the magnetic field is parallel to the principal axis of magnetization.

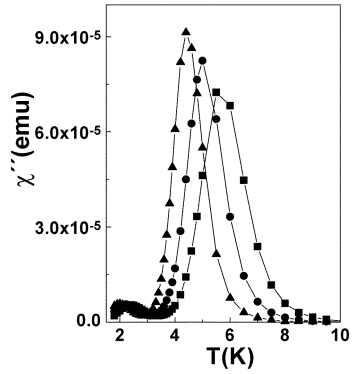

Fig. 5 Plots of χ_M'' *vs.* temperature for complex **2** in an ac field of 1 Oe oscillating at 50 Hz (▼), 250 Hz (●) or 1000 Hz (■).

The plots of the out-of-phase susceptibility χ_M'' signal *versus* temperature at three different frequencies are shown in Fig. 5 for complex **2**. Both complexes exhibit frequency-dependent out-of-phase ac signals in the range of 4–7 K.

Magnetization relaxation times (τ) are obtained from the relationship $\bar{\omega}\tau = 1$ at the maxima of the χ_M'' *vs.* temperature curves, where $\bar{\omega}$ is the frequency of the measurement.[25] The χ_M'' peak positions were determined by fitting the χ_M'' *vs.* temperature data to a Lorentzian function. For the three complexes, the magnetization relaxation rate ($1/\tau$) of the peaks follows the Arrhenius equation. This is the characteristic behavior for a thermally activated Orbach process, the theoretical eqn. (1) for which is given as follows:

$$\frac{1}{\tau} = \frac{1}{\tau_0}\exp(-U_{eff}/kT) \quad (1)$$

In these equations U_{eff} is the effective anisotropy energy barrier, k is the Boltzmann constant and T is temperature. The least-squares fit of the ac susceptibility relaxation data for complexes **2** and **3** gave energy barriers of 65.4 K and 64.4 K, (attempt frequencies $\tau_0 = 2.43 \times 10^{-9}$ and 1.48×10^{-9} s), respectively.

Mass spectrometry. The mass spectra of complexes **2–5** have been recorded.[26] In the matrix-assisted laser desorption/ionization time-of-flight mass spectrometry (MALDI-TOF MS) experiments, the sample of interest combined with a hundred fold (minimum) excess of matrix (most typically an aromatic acid) which absorbs the laser light and subsequently ionises the sample molecule which it surrounds. Only in the case where the complex has an absorption at the wavelengths of the laser source can the mass spectrum be recorded without a matrix (this technique is referred to as laser desorption/ionisation time-of-flight mass spectrometry, LDI-TOF MS). Since the Mn_{12} clusters in this study absorb at the wavelength of the laser light used in the TOF MS instrument employed (see experimental section), mass spectra of complexes **2–5** were recorded both with and without a matrix under different experimental conditions, in search of optimum conditions for the characterisation of this family of compounds.

The high mass region (above 700 Da) LDI-TOF mass spectrum of the complex $[Mn_{12}O_{12}(O_2CC_6H_5)_{16}(H_2O)_4]$ (**4**), recorded in *positive mode* (Fig. 6, upper panel), reveals no peak corresponding to the molecular ion but does show a series of peaks corresponding to the $[Mn_{12}O_{12}(O_2CC_6H_5)_{14}]^+$ ion at $m/z = 2547$ and fragments of it resulting from the stepwise loss of several $C_6H_5CO_2$ units ($\Delta m/z = 121$). Additionally a broad distribution of ions is observed in the 3000–4000 Da mass range, which presumably result from the fusion of metastable ions. In the low-mass region of the spectrum (below 700 Da) a series of peaks, which could not be directly assigned to fragmentations involving the presence of the benzoate anion,

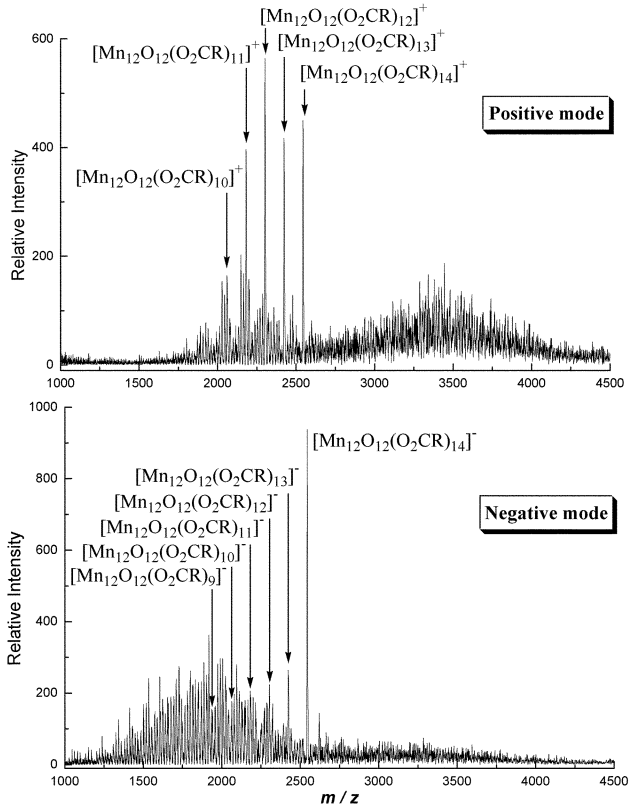

Fig. 6 High mass region of the LDI-TOF mass spectra of complex $[Mn_{12}O_{12}(O_2CC_6H_5)_{16}(H_2O)_4]$ (**4**).

are observed. Furthermore, the most significant peaks in this part of the spectrum are common to all the clusters that have been studied. These fragments may arise from rearrangement of the original cluster, and their explanation must involve the presence of manganese, oxygen and carbon atoms.

In the high-mass region of the LDI-TOF mass spectrum (above 700 Da) recorded in *negative mode* (Fig. 6, lower panel), an intense peak at $m/z = 2547$ attributable to the $[Mn_{12}O_{12}(O_2CC_6H_5)_{14}]^-$ ion is also observed, and no significant ions resulting from cluster fusion are witnessed. Thereafter, the fragmentation of the cluster leads to an extremely complicated pattern, with principle mass differences between the ions of 16 Daltons, corresponding to the loss *or gain* of oxygen atoms to the fragment ions. The low mass region of the *negative mode* spectrum (Fig. 7) is dominated by peaks at $m/z = 714$ and 417, corresponding to the $[Mn_2(O_2CC_6H_5)_5]^-$ and $[Mn(O_2CC_6H_5)_3]^-$ ions, respectively. Peaks assignable to the benzoate (m/z 121.1), $Mn_2O_6^-$ (m/z 205.7) and permanganate (m/z 118.8) anions are also observed, the latter being a general feature of the spectra recorded in *negative mode* for all the clusters.

Spectral features similar to those seen for complex **4** have been observed in the LDI-TOF mass spectra of the complex $[Mn_{12}O_{12}(O_2CCHCHCH_3)_{16}(H_2O)_4]\cdot H_2O$ (**2**). The *negative-ion mode* spectrum of a neat deposit displays two intense peaks at $m/z = 310$ and 535 Daltons, which are attributed to $[Mn(O_2CCHCHCH_3)_3]^-$ and $[Mn_2(O_2CCHCHCH_3)_5]^-$ fragment-ions, respectively. In the 1600–2300 Dalton region there is a series of peaks regularly spaced by $m/z = 85$, corresponding to a crotonate anionic ligand. Finally, in the high-mass region the most intense peak appears at $m/z = 2042$, which is attributed to a $[Mn_{12}O_{12}(O_2CCHCHCH_3)_{14}]^-$ fragment, as well as other less intense peaks at 2127 and 1957 associated with the $[Mn_{12}O_{12}(O_2CCHCHCH_3)_{15}]^-$ and $[Mn_{12}O_{12}(O_2CCHCHCH_3)_{13}]^-$ ions, respectively. The LDI-TOF mass spectra recorded in *positive-ion mode* reveals a dramatic increase of the ionic current. The most intense peak of the spectrum corresponds to the $[Mn_{12}O_{12}(O_2CCHCHCH_3)_{14}]^+$ fragment ion, followed by peaks corresponding to fragments with 12 or 11 carboxylate ligands. However, in the case of complexes $[Mn_{12}O_{12}(O_2CC_6H_4C_6H_5)_{16}(H_2O)_4]\cdot 2C_6H_5C_6H_4COOH$ (**3**) and $[Mn_{12}O_{12}(O_2C\text{-}2\text{-}F\text{-}C_6H_4)_{16}(H_2O)_4]$ (**5**), peaks corresponding to the intact cluster were ***not*** observed. In the *negative mode*, the neat samples all showed peaks resulting from the $[Mn_2(O_2CR)_5]^-$ and $[Mn(O_2CR)_3]^-$ ions.

In order to try and optimize the characterisation conditions for this family of clusters, we also recorded the MALDI-TOF mass spectra. Benzoic acid matrices have been extensively used in MALDI-TOF MS experiments.[13,14] However, in the present case, the use of such matrices may complicate the characterization of the samples since a ligand substitution reaction with the corresponding carboxylic acid of the cluster may take place.[24] For this reason, in the present study the basic 2-amino-4-methyl-5-nitropyridine (AMNP), the neutral 9-nitroanthracene (9NA) and the slightly acidic dithranol have been used as matrices for the clusters. The different MALDI-TOF mass spectra of the complexes were registered both in the *positive* and the *negative mode*.

In the case of **2**, the use of AMNP as matrix gave the highest ionic current in the region corresponding to Mn_{12}-based ions, although the spectrum is considerably more complicated than that recorded in the absence of a matrix. A group of fragments of the general formula $[Mn_{12}O_{12}(O_2CCHCHCH_3)_n]^z$ ($n = 16$–9, $z = +$ or $-$) corresponding to the loss of the anion from the parent cluster are clearly observed. However, the most

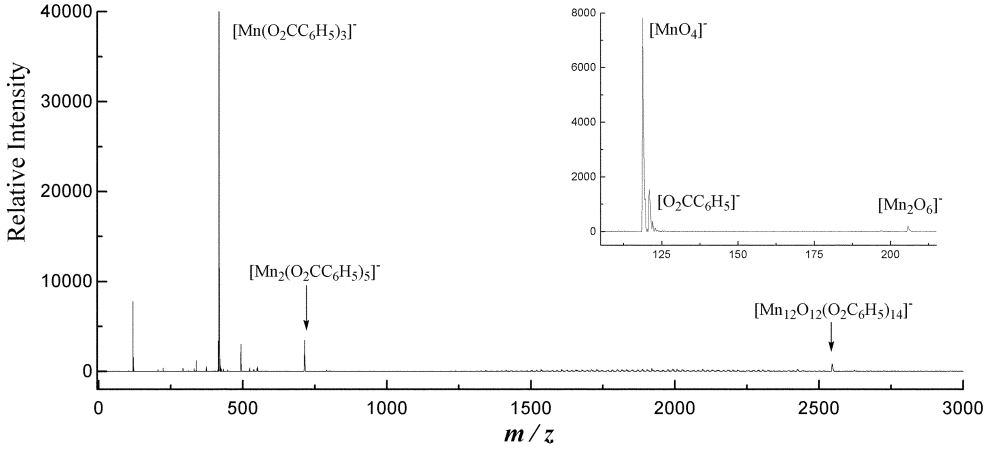

Fig. 7 Full mass range of the negative mode LDI-TOF mass spectra of complex $[Mn_{12}O_{12}(O_2CC_6H_5)_{16}(H_2O)_4]$ (**4**) and (inset) a detail of the low mass region.

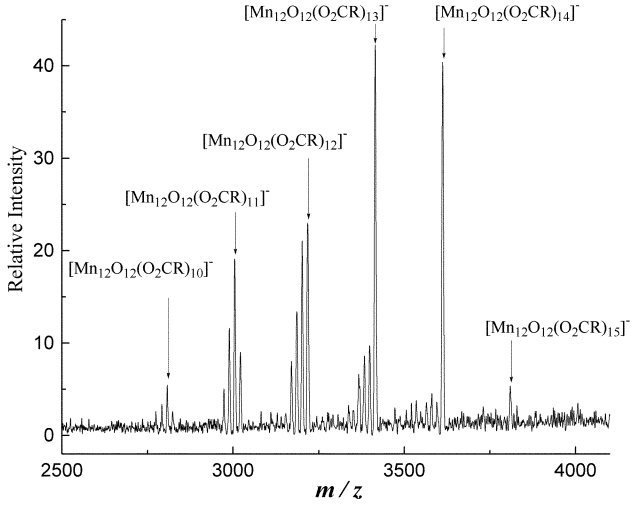

Fig. 8 High mass region of the negative mode MALDI-TOF mass spectra of complex $[Mn_{12}O_{12}(O_2CC_6H_4C_6H_5)_{16}(H_2O)_4]\cdot 2C_6H_5C_6H_4$-COOH (**3**) (9NA matrix).

striking feature is the appearance of a second series of signals arising from the systematic loss *and gain* of oxygen atoms.

In contrast to the results found for complex **2**, the use of AMNP as a matrix did not improve the quality of the LDI-TOF spectra of complex **3**, and again no peaks corresponding to the intact cluster were observed. On the contrary, the best spectra were obtained using 9-NA as a matrix and working in the negative-ion mode. As can be seen in Fig. 8, in such a case a nice doubly periodic patterned spectrum was recorded in the region corresponding to ions with the Mn_{12} core intact.

Finally, the benzoate derivative $[Mn_{12}O_{12}(O_2CC_6H_5)_{16}$-$(H_2O)_4]$ (**4**) yielded good quality mass spectra independently of the matrix and polarity used. Be that as it may, the best conditions were found using AMNP as the matrix in the *positive-ion mode*. In contrast, the best conditions for complex $[Mn_{12}O_{12}(O_2C$-2-F-$C_6H_4)_{16}(H_2O)_4]$ (**5**) (which gave *no* intact cluster ions in LDI-TOF MS) were also found using AMNP as a matrix (with 9NA giving acceptable spectra) but working in the *negative-ion mode* (Fig. 9), in which the characteristic signal of the $[Mn_{12}O_{12}(O_2Co$-$FC_6H_6)_{14}]^-$ ion is clearly observed, the other characteristics being similar to those of the other *negative ion spectra*.

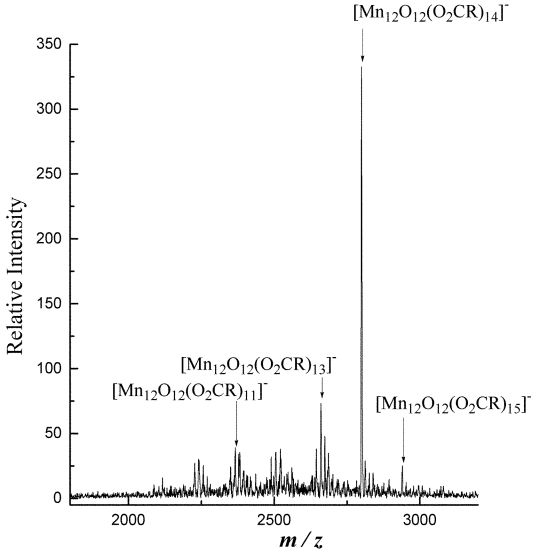

Fig. 9 High mass region of the negative mode MALDI-TOF mass spectra of complex $[Mn_{12}O_{12}(O_2C$-2-F-$C_6H_4)_{16}(H_2O)_4]$ (**5**) (AMNP matrix).

Discussion

The objective of the mass spectrometric study was to assess the applicability of the method for the determination of the molecular composition of dodecanuclear manganese clusters. Therefore, the ideal scenario would be the observation in the spectra of a peak associated with the molecular ion. The observation of such a peak has not been possible, although the characterization of a given complex may be achieved by a detailed analysis of the other of peaks observed under various experimental conditions. It is instructive to hypothesize about the origin of the ions observed. As a general characteristic, the most abundant and clearly identified fragments found in the *negative-ion* MALDI-TOF mass spectra of complexes **2–5**, either as neat samples or in the presence of a matrix, are the $[Mn(O_2CR)_3]^-$ and $[Mn_2(O_2CR)_5]^-$ anions. Surprisingly, the $[Mn^{II}_x(O_2CR)_{(2x\,-\,1)}]^+$ fragments species were not observed in the corresponding *positive mode* spectra. Given the mass-to-charge ratio of the ions, it seems clear that the manganese ions in these fragments are in their +2 oxidation state probably due to laser-induced reactions leading to reduction of the original mixed-valence Mn^{III}/Mn^{IV} complex. Considering that these fragments are also observed in the absence of matrix, a reduction of the manganese centres involving the carboxylate ligands may be involved. This idea is supported by considering the well known ability of Mn^{III} to oxidize carboxylic substrates in organic oxidation reactions,[27] where the thermal reduction of Mn^{III} centres involves an oxidative decarboxylation of a ligand leading to the formation of a Mn^{II} complex, an organic radical and CO_2 (eqn. 2)

$$X_2Mn^{(III)}O_2CR \rightarrow Mn^{(II)}X_2 + CO_2 + R^{\cdot} \qquad (2)$$

The relatively low intensity of the carboxylate ions in the *negative mode* spectra (when compared with the $[Mn(O_2CR)_3]^-$ ion intensity) also supports such a hypothesis. Thus, considering the thermal and electronic activation afforded by the UV laser pulse, an overall fragmentation mechanism involving an oxidative decarboxylation of the ligands located at the periphery of the cluster is proposed (eqn. 3).

$$[Mn^{(III,IV)}_{12}O_{12}(O_2CR)_{16}] \rightarrow [Mn^{(II)}(O_2CR_3)]^- + [Mn^{(II)}_2(O_2CR)_5]^- + CO_2 + R^{\cdot} + MnO_4^- \qquad (3)$$

The remaining manganese and oxygen atoms probably lead to the formation of permanganate anions, although the formation of other species such as MnO or MnO_2, may not be ruled out. Even though such species may be formed, it is not possible to observe them either in the positive or negative mode spectra due to their neutral charge.

Focusing on the high-mass region of the spectra, which contain ions corresponding to clusters with all the twelve Mn ions present, the fragmentation of the clusters produces nice patterns of peaks in which the $[Mn_{12}O_{12}(O_2CR)_n]^z$ (n = 14 or 13, z = + or −) ions are the most abundant species. Moreover, these patterns very often exhibit a double periodicity, especially as the number of lost carboxylate anions increases. Indeed, the intensity of the peaks increases rapidly from the parent peak of the $[Mn_{12}O_{12}(O_2CR)_{16}]$ species to the $[Mn_{12}O_{12}(O_2CR)_n]^z$ fragment ions where n = 13 or 14. From here on, the intensity of the peaks decreases to n = 9 giving a shape reminiscent of a statistical distribution. The second period of peaks corresponds, on average, to the loss or gain of oxygen atoms for a given fragment. Interestingly, the same fragments are observed in both *negative-* and *positive-ion modes*, and fragments corresponding to the loss of more than one carboxylate ligand, which in the absence of other redox processes should give ions with a net total charge (Z) greater than one, are apparently singly charged. These observations indicate that the

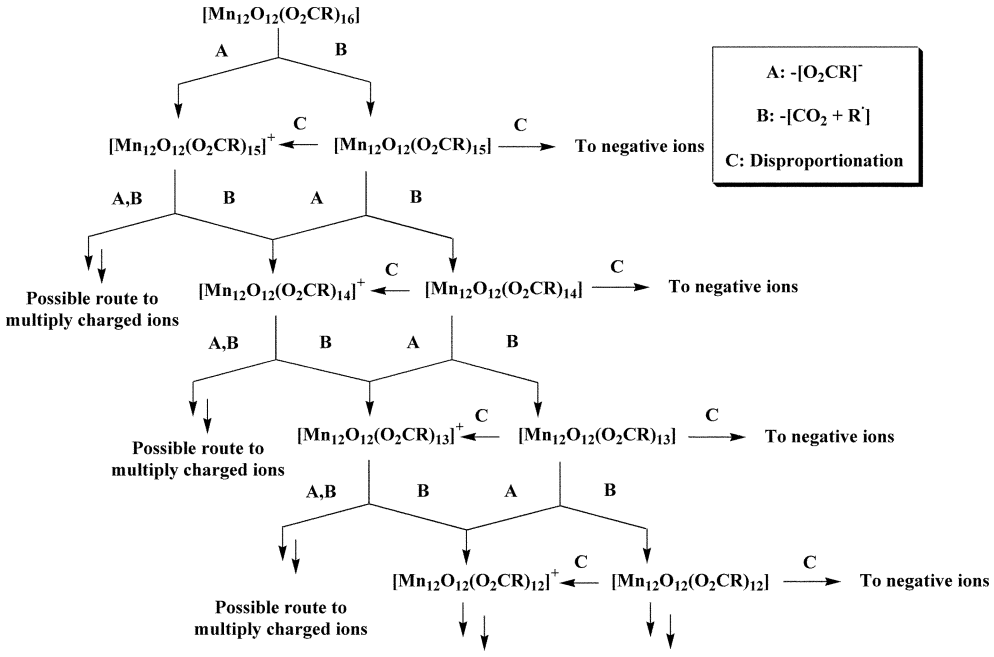

Scheme 2

formation of the Mn_{12} fragments may occur following at least two different pathways. As depicted in Scheme 2, starting from the parent $[Mn_{12}O_{12}(O_2CR)_{16}]$ fragment, the first pathway involves the loss of a carboxylate anion (process A) leading to the formation of $[Mn_{12}O_{12}(O_2CR)_{15}]^+$ which is observed in the *positive-ion mode* spectra. Following the second path, an oxidative ligand decarboxylation process (B) leads to the formation of the neutral $[Mn_{12}O_{12}(O_2CR)_{15}]$ fragment, in which one of the Mn(III) ions in the original cluster is reduced to Mn(II). Losing a carboxylate anion, the neutral fragment $[Mn_{12}O_{12}(O_2CR)_{15}]$ gives the positively charged $[Mn_{12}O_{12}(O_2CR)_{14}]^+$ fragment ion (process A). The oxidative decarboxylation route B of $[Mn_{12}O_{12}(O_2CR)_{15}]^+$ also leads to $[Mn_{12}O_{12}(O_2CR)_{14}]^+$, and so on. Alternatively, the neutral $[Mn_{12}O_{12}(O_2CR)_{15}]$ undergoing a disproportionation process (C) could explain the formation of $[Mn_{12}O_{12}(O_2CR)_{15}]^+$, as well as the negative ions that are formed (*vide infra*). As the ligands around the clusters are peeled off, new highly reactive species are formed (Scheme 2), which could react with reduced neutral complexes to form new positive fragments (eqn. 4). Such a process could also explain the formation of ions at higher masses, corresponding to fused clusters, as seen in the LDI spectra in Fig. 6.

The oxidation states of the manganese ions in these species clearly departs from the original $Mn(III)_8Mn(IV)_4$ composition, and, in line with the electrochemical behaviour of the clusters, it seems logical that the first steps involve reduction of the Mn(III) to Mn(II).

$$[Mn_{12}O_{12}(O_2CR)_n]^{2+} + [Mn_{12}O_{12}(O_2CR)_m] \rightarrow [Mn_{12}O_{12}(O_2CR)_n]^{+} + [Mn_{12}O_{12}(O_2CR)_m]^{+} \quad (4)$$

The most likely sources of the fragment ions observed in the *negative-ion mode* spectra are either from a disproportionation of neutral fragments or from the coordination of additional carboxylate and/or oxide anions onto a neutral or singly positively charged complex (as observed in the low- and high-mass areas of the negative-ion mode spectra)(Scheme 3). In the first case a neutral fragment $[Mn_{12}O_{12}(O_2CR)_n]$ originating from an oxidative decarboxylation disproportionates into two ions, $[Mn_{12}O_{12}(O_2CR)_n]^-$ and $[Mn_{12}O_{12}(O_2CR)_n]^+$, thus giving another possible source for the positive ions. Following this disproportionation, an oxidative decarboxylation of $[Mn_{12}O_{12}(O_2CR)_n]^-$ gives rise to $[Mn_{12}O_{12}(O_2CR)_{n-1}]^-$ and so on. In the second case, coordination of a carboxylate anion to the overall neutral $[Mn_{12}O_{12}(O_2CR)_n]$ cluster would lead to the $[Mn_{12}O_{12}(O_2CR)_{n+1}]^-$ species, an occurrence which may

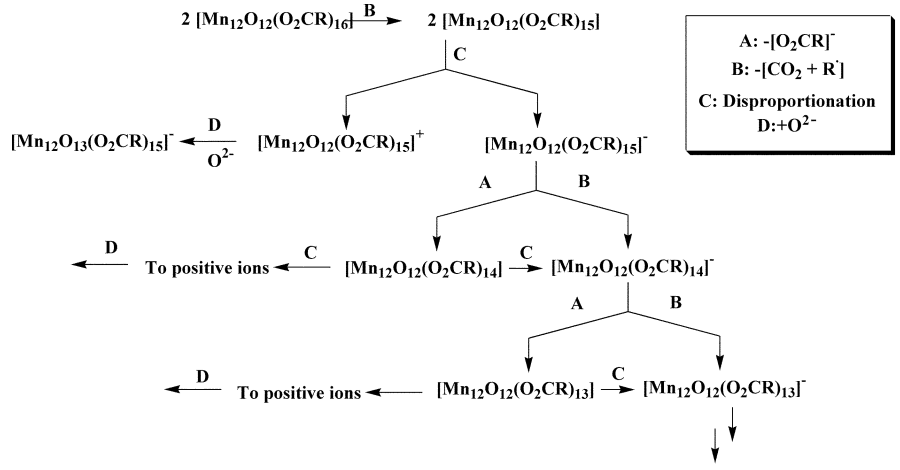

Scheme 3

explain the observation of the molecular peak in some of the spectra obtained in the negative-ion mode. Alternatively, coordination of an oxide anion (D in Scheme 3) to a positively charged or neutral fragment would lead to negative ions. This type of oxide crossing pathway would explain the observation of ions of mass greater than the molecular ion in the case of the cluster with crotonate as anion. It interesting to note that neither in the *positive* nor the *negative mode* are the peaks corresponding to the clusters with the four H_2O ligands observed. The H_2O molecules are presumably lost under the high vacuum conditions used for the experiments.

Conclusions

Two new Mn_{12} SMMs have been synthesized and characterized. The structural characterization of complex **2** reveals that the complex possesses the $[Mn_{12}(\mu_3\text{-}O)_{12}]$ core comprising a central $[Mn^{IV}{}_4O_4]^{8+}$ cubane unit held within a nonplanar ring of eight Mn^{III} ions by eight $\mu_3\text{-}O^{2-}$ ions, characteristic of $[Mn_{12}O_{12}(O_2CR)_{16}(H_2O)_4]$ complexes. Both new complexes **2** and **3** show an out-of-phase ac magnetic susceptibility χ_M'' signal in the 4–7 K region and magnetization hysteresis loops characteristic of single-molecule magnets. LDI- and MALDI-TOF mass spectrometry of both complexes together with those of other previously reported Mn_{12} complexes, confirm the potential utility of this spectrometric technique for measuring the molecular weights of the family of Mn_{12} clusters. Three main factors govern the observation (or not) of intact cluster ions in MALDI-TOF experiments: i) the photochemical and redox properties of the analyte (especially for the LDI spectra); ii) the effectiveness of the matrix in ionizing the analyte, and iii) the stability of the ions formed by the analyte. Mn_{12} clusters have a rich electrochemistry, which leads to the observation of positive and negative ions in which the core of the molecule is intact, but presumably with varying degrees of oxidation state (from Mn(*IV*) to Mn(*II*)) according to the number of carboxylate counter-ions that are ejected. With respect to point (ii), the ability of the matrix to aid in the observation of molecular ions is usually associated with the capability to form crystallites incorporating the analyte. Given this hypothesis, it is not strange that for the complexes with crotonate or benzoate ligands AMNP is the best matrix, whereas for the cluster with the phenyl-4-benzoate ligand it is 9NA. It should be emphasised that the use of matrix is *essential* for the observation of cluster ions of **3** and **5** in which the core of the molecules is intact. Thus, generally speaking, although it was possible in some cases to generate and detect Mn_{12} complexes fragment ions without using a matrix, its presence appeared to be essential to prevent molecular ion decomposition, and is beneficial for obtaining good signal-to-noise ratio in the spectra. We are presently employed in establishing the generality of the MALDI-TOF MS in this family of SMMs.

Acknowledgement

G. C. and D. N. H thank the National Science Foundation for its financial support. J. V. thanks the DGI (project MAT2000–1388-C03–01), DGR (project 2000 SGR 00114) and Cooperación Bilateral Hispano-Americana (Spanish Government). The magnetic susceptibility measurements were performed with an MPMS2 SQUID magnetometer provided by the Center for Interface and Material Science, funded by the W. M. Keck Foundation. D. R.-M. is grateful to the Ministerio de Ciencia y Tecnología (Spanish Government) for a postdoctoral contract. P. G. is grateful to the 3MD TMR Network of the European Union for a postdoctoral contract.

References

1 (*a*) D. A. Garanin and E. M. Chudnovsky, *Phys. Rev. B.*, 1997, **56**, 11102; (*b*) E. M. Chudnovsky, *Science*, 1996, **274**, 938; (*c*) G. P. Berman, G. D. Doolen, D. Holm and V. L. Tsifrinovich, *Phys. Lett. A.*, 1994, **193**, 444; (*d*) L. Gunther, *Physics World*, 1990, December 28.

2 (*a*) See for example: R. F. Ziolo, E. P. Giannelis, M. P. O. Weinstein, B. N. Ganguly, V. Mehrotra, M. W. Russell and D. R. Huffman, *Science*, 1992, **257**, 219.

3 (*a*) E. D. Dahlberg and J. G. Zhu, *Physics Today*, 1995, 34; (*b*) R. D. Michael, R. D. Shull, L. J. Swartzebdruber, J. H. Bennet and R. E. Watson, *J. Magn. Magn. Mater.*, 1992, **111**, 29; (*c*) D. D. Awschalom, D. P. Divicenzo and F. F. Smyth, *Science*, 1992, **258**, 414; (*d*) D. Loss, D. P. DiVicenzo and G. Gunstein, *Phys. B.*, 1993, **189**, 189; (*e*) E. M. Chudnovsky, *J. Magn. Magn. Mater.*, 1995, **140**, 1821.

4 (*a*) R. Sessoli, D. Gatteschi, A. Caneschi and M. Novak, *Nature*, 1993, **365**, 149; (*b*) R. Sessoli, H. -K. Tsai, A. R. Schake, S. Wang, J. B. Vincent, K. Folting, D. Gatteschi, G. Christou and D. N. Hendrickson, *J. Am. Chem. Soc.*, 1993, **115**, 1804.

5 (*a*) J. R. Friedman, M. P. Sarachik, J. Tejada, J. Maciejewski and R. Ziolo, *J. Appl. Phys.*, 1996, **79**, 6031; (*b*) J. R. Friedman, M. P. Sarachik, J. Tejada and R. Ziolo, *Phys. Rev. Lett.*, 1996, **76**, 3830; (*c*) J. R. Friedman, Ph. D. Thesis, 1996, The City College of New York, New York City, N.Y., U.S.A.; (*d*) L. Thomas, F. Lionti, R. Ballou, D. Gatteschi, R. Sessoli and B. Barbara, *Nature*, 1996, **383**, 145.

6 (*a*) D. Ruiz, Z. Sun, S. M. J. Aubin, E. Rumberger, C. Incarvito, K. Folting, A. L. Rheingold, G. Christou and D. N. Hendrickson, *Mol. Cryst. Liq. Cryst.*, 1999, **335**, 413; (*b*) S. M. J. Aubin, D. Ruiz, E. Rumberger, Z. Sun, B. Albela, M. Wemple, N. R. Dilley, J. Ribas, M. B. Maple, G. Christou and D. N. Hendrickson, *Mol. Cryst. Liq. Cryst.*, 1999, **335**, 371.

7 (*a*) D. Ruiz-Molina, G. Christou and D. N. Hendrickson, in *Hyper-Structured Materials*, Gordon-Breach publishers, in press; (*b*) D. Ruiz-Molina, G. Christou and D. N. Hendrickson, *Mol. Cryst. Liq. Cryst.*, 2000, **343**, 17.

8 (*a*) H. L. Tsai, H. J. Eppley, N. Devries, K. Folting, D. N. Hendrickson and G. Christou, *Chem. Commun.*, 1994, **15**, 1745; (*b*) S. M. J. Aubin, S. Spagna, H. J. Eppley, R. E. Sager, G. Christou and D. N. Hendrickson, *Chem. Commun.*, 1998, 803; (*c*) S. M. J. Aubin, Z. Sun, L. Pardi, J. Kryzstek, K. Folting, L. C. Brunel, A. L. Rheingold, G. Chrtistou and D. N. Hendrickson, *Inorg. Chem.*, 1999, **38**, 6329; (*d*) K. Takeda, K. Awaga and T. Inabe, *Phys. Rev. B.*, 1998, **57**, 110621.

9 (*a*) S. M. J. Aubin, N. R. Dilley, M. W. Wemple, M. B. Maple, G. Christou and D. N. Hendrickson, *J. Am. Chem. Soc.*, 1998, **120**, 839; (*b*) S. M. J. Aubin, N. R. Dilley, L. Pardi, J. Kryzstek, M. W. Wemple, L. C. Brunel, M. B. Maple, G. Christou and D. N. Hendrickson, *J. Am. Chem. Soc.*, 1998, **120**, 4991.

10 E. K. Brechin, J. Yoo, M. Nakano, J. C. Huffman, D. N. Hendrickson and G. Christou, *Chem. Commun.*, 1999, 783.

11 (*a*) Z. Sun, C. M. Grant, S. L. Castro, D. N. Hendrickson and G. Christou, *Chem. Commun.*, 1998, 721; (*b*) S. L. Castro, Z. Sun, C. M. Grant, J. C. Bollinger, D. N. Hendrickson and G. Christou, *J. Am. Chem. Soc.*, 1998, **120**, 2365.

12 (*a*) A. -L. Barra, P. Debrunner, D. Gatteschi, C. E. Schulz and R. Sessoli, *Europhys. Lett.*, 1996, **35**, 133; (*b*) C. Sangregorio, T. Ohm, C. Paulsen, R. Sessoli and D. Gatteschi, *Phys. Rev. Lett.*, 1997, **78**, 4645.

13 (*a*) For general discussions concerning MALDI-TOF MS, see: F. Hillenkamp, M. Karas, R. C. Beavis and B. T. Chait, *Anal. Chem.*, 1991, **63**, 1193A–1202A; (*b*) *Time-of-flight Mass Spectrometry*, R. J. Cotter, (Ed.); American Chemical Society Symposium Series 549: Washington DC, 1994; (*c*) K. O. Börnsen, *Anal. Methods Instrum.*, 1995, **2**, 202; (*d*) M. Karas, M. Glückmann and J. Schäfer, *J. Mass Spectrom.*, 2000, **35**, 1–12.

14 (*a*) M. Karas and F. Hillenkamp, *Anal. Chem.*, 1988, **60**, 2299–2301; (*b*) K. Tanaka, H. Waki, Y. Ido, S. Akita, Y. Yoshida and T. Yoshida, *Rapid Commun. Mass Spectrom.*, 1988, **8**, 151–153; (*c*) R. J. Cotter, *Time-of-Flight Mass Spectrometry: Instrumentation and Applications to Biological Research*, American Chemical Society, Washington DC, 1997; (*d*) C. Fenselau, *Anal. Chem.*, 1997, **69**, 661A.

15 (*a*) H. J. Räder and W. Schrepp, *Acta Polymer.*, 1998, **49**, 272–293; (*b*) K. J. Wu and R. W. Odom, *Anal. Chem.*, 1998, **70**, 456A.

16 For examples of dendrimer analysis by MALDI-TOF MS, see: (*a*) J. W. Leon, M. Kawa and J. M. J. Fréchet, *J. Am. Chem. Soc.*, 1996, **118**, 8847; (*b*) G. Chessa, A. Scrivanti, R. Seraglia and P. Traldi, *Rapid Commun. Mass Spectrom.*, 1998, **12**, 1533; (*c*) D. Yu,

N. Vladimirov and J. M. J. Fréchet, *Macromolecules*, 1999, **32**, 5186; (*d*) C. Kim and I. Jung, *J. Organomet. Chem.*, 1999, **588**, 9.
17 N. Carter Dopke, P. M. Treichel and M. M. Vestling, *Inorg. Chem.*, 1998, **37**, 1272.
18 G. Critchley, P. J. Dyson, B. F. G. Johnson, J. S. McIndoe, R. K. O'Reilly and P. R. R. Langridge-Smith, *Organometallics*, 1999, **18**, 4090.
19 P. J. Dyson, B. F. G. Johnson, J. S. McIndoe and P. R. R. Langridge-Smith, *Inorg. Chem.*, 2000, **39**, 2430.
20 T. Lis, *Acta Cryst.*, 1980, **B36**, 2042.
21 Z. Sun, D. Ruiz, N. R. Dilley, M. Soler, J. Ribas, I. A. Guzei, A. L. Rheingold, K. Folting, M. B. Maple, G. Christou and D. N. Hendrickson, *Chem Commun.*, 1999, 1973.
22 N. Walker and D. Stuart, *Acta Crystallogr., Sect. A: Fundam. Crytallogr.*, 1983, **39**, 158.
23 E. A. Schmitt and D. N. Hendrickson, unpublished results.
24 G. Aromi, S. M. J. Aubin, M. A. Bolcar, G. Christou, H. J. Eppley, K. Folting, D. N. Hendrickson, J. C. Huffman, R. Squire, H.-L. Tsai, S. Wang and M. W. Wemple, *Polyhedron*, 1998, **17**, 3005.
25 C. Paulsen and J.-G. Park, in *Quantum Tunneling of Magnetization-QTM'94*, eds. L. Gunther and B. Barbara, Kluwer Academic Publishers, Dordrecht, 1995, pp 171–188.
26 In this study, we chose cluster **4** as a "standard", since its precursor, the Mn12Ac (1), has not proven amenable to MALDI-TOF and LDI-TOF MS analyses to the present time. No cluster ions are observed. This result could be due to: 1) the poor solubility of the compound in all solvents, resulting in 2) the absence of good cluster-matrix co-crystals, or 3) the low stability of the ions formed upon irradiation in the MALDI experiment.
27 J. M. Anderson and J. K. Kochi, *J. Am. Chem. Soc.*, 1970, **92**, 2450–2460.